



## Gold supported on ceria doped by $\text{Me}^{3+}$ (Me = Al and Sm) for water gas shift reaction: Influence of dopant and preparation method

Donka Andreeva<sup>a,\*</sup>, Margarita Kantcheva<sup>b</sup>, Ivan Ivanov<sup>a</sup>, Lyuba Ilieva<sup>a</sup>, Janusz W. Sobczak<sup>c</sup>, Wojciech Lisowski<sup>c</sup>

<sup>a</sup> Institute of Catalysis, Bulgarian Academy of Sciences, "Acad. G. Bonchev" str., bl.11, 1113 Sofia, Bulgaria

<sup>b</sup> Department of Chemistry, Bilkent University, 06800 Bilkent, Ankara, Turkey

<sup>c</sup> Institute of Phys. Chem., PAS, Kasprzaka 44/52, 01-224 Warsaw, Poland

### ARTICLE INFO

#### Article history:

Available online 26 June 2010

#### Keywords:

Gold catalysts  
Sm and Al doped ceria  
Preparation methods  
WGS activity and mechanism

### ABSTRACT

Gold catalysts supported on ceria doped by Sm and Al were studied. The influence of the preparation method, as well as the nature of dopants on the structure, properties and WGS activity are investigated. The applied methods of preparation cause the modification of ceria in a different extent. In the sample prepared by co-precipitation (CP) and doped by Al, the vacancies are located within the bulk of ceria structure, whereas in the corresponding AuCeSmCP sample the vacancies are located most likely around Sm and the ceria structure seems to be better ordered than the Al doped ceria. There is no distinct correlation between the reducibility and WGS activity of the studied catalysts. The Au 4f XPS spectra of fresh samples reveal higher contribution of dispersed form of Au for Sm doped catalysts than for the corresponding Al doped samples. The Ce 3d XPS spectra disclose also a higher concentration of  $\text{Ce}^{3+}$  evaluated before the catalytic operation for Sm doped catalysts as compared with the Al doped fresh samples. The observations by "in situ" FT-IR spectroscopy agree well with the model of active sites and the mechanism of the WGS reaction proposed recently by some of us. The amount of formate species observed on the AuCeSmCP is higher than that on the AuCeAlCP catalyst and parallels the catalytic activity. The higher concentration of active sites on the surface of the AuCeSmCP catalyst facilitates the dissociation of water.

© 2010 Elsevier B.V. All rights reserved.

### 1. Introduction

Gold catalysts based on ceria are very promising for various applications and among them the pure hydrogen production via water gas shift (WGS) reaction is of great importance. Recently, the interest in WGS is increasing because of its potential application in the fuel cell technology. The application of the WGS gold catalysts to fuel cell power systems requires high catalytic activity and stability in cyclic operation. In the last few years gold catalysts supported on ceria and on ceria doped by different  $\text{Me}^{3+}$  were studied intensively in our group [1–3]. It is well known that ceria is an appropriate support for precious metals, due to its high oxygen storage capacity (OSC). Luo et al. have found a direct relationship between the WGS activity and the OSC [4]. Metal-modified ceria has higher oxygen capacity and enhanced reducibility than pure ceria. The addition of metal dopants having valences lower than (4+) leads to the formation of oxygen vacancies in ceria, which is expected to increase the redox activity.

Recently, Panagiotopoulou and Kondarides have investigated the effect of support nature on the catalytic performance of noble metal catalysts for the WGS reaction [5], as well as the WGS activity of metal doped Pt/CeO<sub>2</sub> catalysts [6]. They concluded that the WGS activity of Pt and Ru catalysts does not depend on the metal loading and dispersion of crystallite size, but depends strongly on the nature of metal oxide carrier [5]. They have also studied the influence of the doped Pt/CeO<sub>2</sub> catalysts by different metals (Ca, La, Mg, Zn, Zr, Yb, Y, and Gd) and have established that the catalytic activity in WGS depends on the nature of the dopant employed [6]. The effect of support on the reactivity of gold-based catalysts was also analyzed by Chen and Goodman [7]. The authors considered the multi-role support effect in activating nanosized Au particles including the source for nucleating sites and/or charge transfer, directly related to the reactants and their activation. This concept fully confirms our suggestion, based on experimental data analysis, about the active role of ceria as support for nanosized gold particles [2,3,8]. The nature of the support plays a decisive role on the distribution and dynamics of oxygen vacancies as well as on the dispersion and shape of gold nanoparticles, which influences directly the catalytic activity.

\* Corresponding author.

E-mail address: [andreev@ic.bas.bg](mailto:andreev@ic.bas.bg) (D. Andreeva).

The addition of  $\text{Me}^{3+}$  dopants to ceria may have two consequences: first—to increase the number of oxygen vacancies in ceria structure and second—to improve the thermal stability of the catalysts by hindering the aggregation of gold and ceria. In the present study we performed a comparative analysis regarding these points using as examples gold catalysts supported on ceria doped by Al and Sm. The nature of the dopants and their influence on the structure and properties of the supports, as well as on the WGS activity, are discussed.

## 2. Experimental

### 2.1. Catalysts preparation

The supports were prepared using two different methods in which ceria was modified by the addition of alumina and samarium oxide. The first synthesis route involved the co-precipitation of ceria and corresponding dopants' hydroxides from metal nitrate solutions, taken in a desired ratio, with a solution of  $\text{K}_2\text{CO}_3$  at constant pH 9.0 and temperature = 60 °C. The resulting precipitates were aged at the same temperature for 1 h, then filtered and washed until the removal of  $\text{NO}_3^-$  ions. The washed precipitates were dried in vacuum at 80 °C and calcined under air at 400 °C for 2 h. The content of dopant in the mixed supports was 10 wt%. The supports prepared in this way are denoted as CP. The second set of mixed  $\text{CeO}_2$ – $\text{Me}_2\text{O}_3$  supports was prepared by mechanically mixing of the corresponding metal oxides and vacuum dried cerium hydroxide, following the procedure described in [1]. The mixture was mechano-chemically activated by milling for 30 min in a mortar followed by calcination at 400 °C for 2 h. The content of dopant was also 10 wt% and the supports prepared in this way are denoted as MA. The gold (2 wt%) was deposited as  $\text{Au}(\text{OH})_3$  on the oxide supports, preliminarily suspended in water, under full control of all parameters of preparation. However, prior to the gold hydroxide deposition, the mixed oxide support was activated in a UV disintegrator under vigorous stirring. After filtering and careful washing, the precursors were dried under vacuum and finally calcined at 400 °C for 2 h. Sample of gold, deposited on pure ceria, was also prepared and denoted as AuCe. The samples using the CP supports are denoted as AuCeAlCP and AuCeSmCP. Samples using the MA supports are denoted as AuCeAlMA and AuCeSmMA.

### 2.2. Catalysts characterization

The BET surface area of the samples was determined on a 'Flow Sorb II-2300' device.

The X-ray diffraction measurements were performed by an automatic powder diffractometer DRON (Bragg–Brentano arrangement), using  $\text{Cu K}\alpha_1$  radiation and a scintillation counter. The diffraction patterns were recorded in a step-scan mode with a step of  $0.02^\circ$  ( $2\theta$ ), counting time 1 s, in the angular interval  $20$ – $90^\circ$  ( $2\theta$ ). The Powder Cell program [9] was used for diffraction data processing.

The Raman spectra were recorded using a SPEX 1403 double spectrometer with a photomultiplier, working in the photon counting mode. The 488 nm line of an  $\text{Ar}^+$  ion laser was used for excitation. The laser power on the samples was 60 mW. The samples were prevented from overheating during the measurements by increasing the size of the focused laser spot. The optimal conditions were chosen, checking the intensity, position and the full width at half maxima (FWHM) of the  $464\text{ cm}^{-1}$  Raman line of  $\text{CeO}_2$ . The spectral slit width was  $4\text{ cm}^{-1}$ . The FWHM of the main Raman line of ceria was calculated.

The TPR measurements were performed on a device described elsewhere [10]. A cooling trap ( $-40^\circ\text{C}$ ) for removing water formed

during reduction was mounted in the gas line prior to the thermal conductivity detector. A hydrogen–argon mixture (10%  $\text{H}_2$ ), dried over a molecular sieve 5A ( $-40^\circ\text{C}$ ), was used to reduce the samples at a flow rate of  $24\text{ ml min}^{-1}$ . The temperature was linearly raised at a rate of  $15^\circ\text{C min}^{-1}$ . The sample mass used was 0.05 g. It was selected by the criterion proposed by Monti and Baiker [11]. In addition, TPR experiments after reoxidation were performed. The reoxidation with purified air was carried out at  $200^\circ\text{C}$  just after the end of the first TPR peak of the fresh sample. The sample was kept in air at this temperature for 15 min and the TPR profiles were recorded after cooling down to room temperature (RT) under purified argon.

The X-ray photoelectron spectroscopy data were recorded on a VG Scientific ESCALAB-210 spectrometer using Al  $\text{K}\alpha$  radiation (1486.6 eV) from an X-ray source operating at 15 kV and 20 mA. The spectra were collected with analyzer pass energy 20 eV, step 0.1 eV and an electron take off angle of  $90^\circ$ . The samples were pressed into thin wafers and degassed in a preparation chamber before analysis. The Shirley background subtraction and peak fitting with Gaussian–Lorentzian product peak was performed using a XPS processing program Advantage (Thermo Electron Corporation). The charging effects were corrected by adjusting the  $\text{Ce } 3d_{3/2}$  peak, usually described as  $u'''$  peak to a position of 917.00 eV [12–14]. This is a strong, individual peak and its position can be established much more precisely than that of the commonly used C 1s peak from adventitious carbon.

The FT-IR spectra were recorded on a Bomem MB 102 FT-IR spectrometer equipped with a liquid-nitrogen cooled MCT detector at a resolution of  $4\text{ cm}^{-1}$  (128 scans). The self-supporting discs ( $0.02\text{ g/cm}^2$ ) were activated in situ. The activation procedure consisted in two steps: (i) treatment of the sample in atmosphere of 100 mbar of oxygen at  $400^\circ\text{C}$  for 1 h, followed by evacuation of oxygen for 30 min at  $150^\circ\text{C}$  and (ii) subsequent exposure of the sample to 10 mbar of hydrogen for 30 min at  $150^\circ\text{C}$  followed by evacuation at the same temperature and cooling to room temperature. The spectrum taken at room temperature after the second step of activation has been used as a background reference (except for the spectra in Fig. 9). The sample spectra are also gas-phase corrected.

### 2.3. Catalytic activity measurements

The catalytic activity of the samples towards the WGS reaction, expressed as the degree of CO conversion, was evaluated over a wide temperature range ( $140$ – $350^\circ\text{C}$ ). The activity was measured in a flow reactor at atmospheric pressure. A gas mixture of initial composition 4.494 vol.% CO in argon was used. The samples were tested in WGS—as prepared and after reoxidation after 1 week operation. The reoxidation was carried out at  $200^\circ\text{C}$  for 1 h in air, space velocity of air  $2000\text{ h}^{-1}$ .

The WGS reaction was carried out under the following experimental conditions: catalyst bed volume— $0.5\text{ cm}^3$  ( $0.63$ – $0.80\text{ mm}$  sieve fraction), space velocity of the dry gas— $4000\text{ h}^{-1}$ , partial pressure of water vapor— $31.1\text{ kPa}$ . The CO content at the reactor outlet was determined using an "Uras 3G" (Hartmann&Braun AG) gas analyzer.

## 3. Results

### 3.1. Catalytic activity

Fig. 1 shows the temperature dependence of CO conversion of the fresh gold catalysts. The following order of activities was observed:

$\text{AuCeSmMA} > \text{AuCeAlMA} > \text{AuCeSmCP} > \text{AuCe} > > \text{AuCeAlCP}$

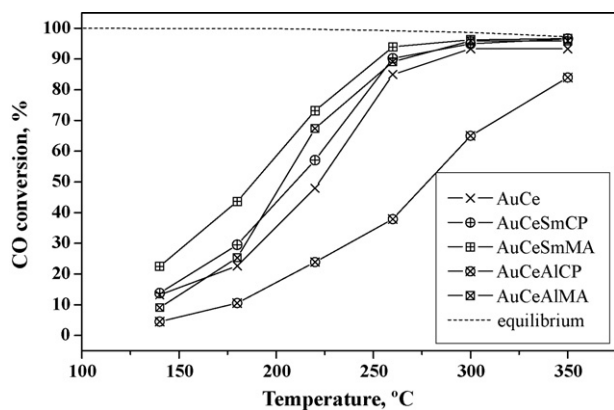


Fig. 1. Temperature dependence of CO conversion of the fresh gold catalysts.

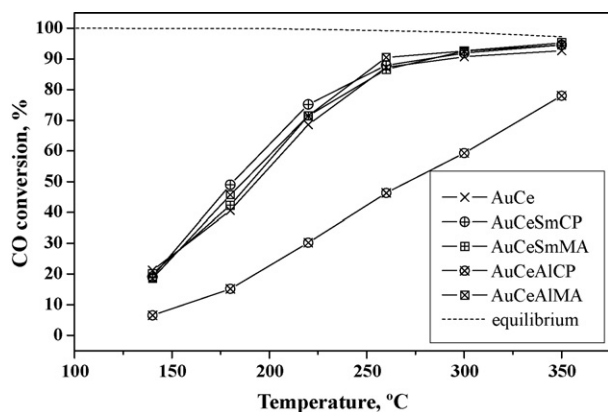


Fig. 2. Temperature dependence of CO conversion of gold catalysts after 1 week of operation and reoxidation in air at 200 °C.

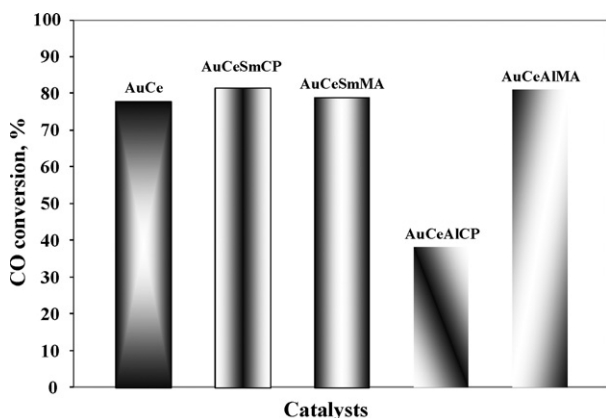


Fig. 3. CO conversion at 240 °C of the re-oxidized catalysts.

Generally, the MA samples are more active than CP ones, although the WGS activity of both types of the catalysts doped by Sm does not differ so much. Significant differences in the catalytic activity are observed for the samples MA and CP modified by Al.

After 1 week of operation and reactivation of the catalysts in air at 200 °C, the WGS activity of the AuCeSmCP catalyst increased even slightly. However, no distinct difference was found for the samples, doped by Sm (compare the WGS activity at 240 °C presented in Figs. 2 and 3). For the catalysts doped by alumina the observed difference in WGS activity was kept. The explanation should be searched in the nature of the used dopants, as well as in the structure and properties of the modified catalysts depending on the preparation methods.

### 3.2. Catalysts characterization

The XRD diffraction patterns of the studied samples are given in Fig. 4. The analysis of the presented data indicates, that the CP catalysts are characterized by a single phase, while in the MA catalysts doped by Sm the double phases can be distinguish: except of the lines of ceria, also the lines of  $\text{Sm}_2\text{O}_3$  are visible. For the Al doped MA sample, the Al lines are not visible. The XRD data allows to calculate both lattice parameters of ceria and average size of gold and ceria. All these parameters and surface areas determined by BET are given in Table 1. The average size of gold in AuCe and Sm containing samples was calculated on the basis of HRTEM data due to the low content and high dispersion of Au [3]. The data collected in Table 1 clearly show that the  $a$  parameter for Sm doped ceria is close to that of the unpromoted ceria and there is no big difference between the  $a$  values for MA and CP samples. On the contrary, in the case of Al doped ceria, the  $a$  parameter for CP sample is lower than other values in Table 1, which corresponds well to the lower ionic radius of  $\text{Al}^{3+}$ . The CP sample doped by Al exhibits also the smallest average size of ceria particles (4 nm). For the other samples studied, the average size of ceria particles is in the order of 7–9 nm.

Fig. 5 shows the Raman spectra of both initial supports and Au containing catalysts. The main line of ceria dominates in all presented spectra. In the spectrum of the CeSmMA sample, the line at  $344\text{ cm}^{-1}$ , typical of  $\text{Sm}_2\text{O}_3$ , is also clearly seen. This is in agreement with the XRD results. The width of the main line of ceria, registered in the Raman spectra, can be considered as indicative of the ceria dispersion and the concentration of oxygen vacancies formed on the defective structure of ceria [15,16]. The FWHM (full width at half maximum) of this line was calculated for all analyzed samples and the data were summarized in Table 2. Comparing these values for the various dopants, one can see that the addition of  $\text{Me}^{3+}$  causes an increase in the FWHM reaching the highest value for the AuCeAlCP sample. It is important to note also that the FWHM value for the AuCeAlMA is much lower than the corresponding value for the AuCeAlCP sample. This is in agreement with our preposition that the oxygen vacancies are deeper in the CP sample, while in the MA sample, the Al dopant modifies only the surface of the catalysts. Quite different relation between the FWHM values can be observed for the Sm doped samples. It is seen that there is no big difference in FWHM values calculated for CP and MA samples and these values are lower than those for both Al doped catalysts. It is likely that in the Sm doped samples, oxygen vacancies are adjusted around Sm atoms and the ceria structure seems to be better ordered.

The results of TPR measurements are presented in Fig. 6. Only the LT TPR profiles are shown, because the HT region is not of impor-

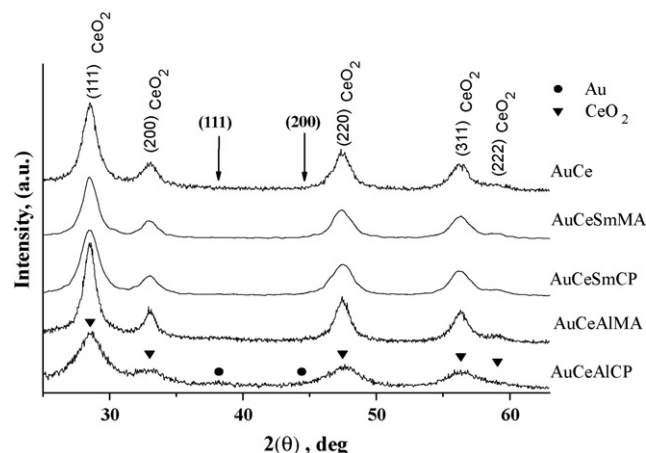


Fig. 4. XRD profiles of the studied catalysts.

**Table 1**  
BET surface area, lattice parameters of ceria and average size of gold and ceria particles.

Samples	$S_{\text{BET}}$ ( $\text{m}^2\text{g}^{-1}$ )	Average size of gold (nm)	Lattice parameter of ceria <sup>a</sup> ( $\text{\AA}$ )	Average size of ceria (nm)
AuCe	108	2.0 <sup>b</sup>	5.422	8.0
AuCeAlCP	103	3.1	5.409	4.2
AuCeAlMA	105	2.9	5.419	9.6
AuCeSmCP	84	2.6 <sup>2</sup>	5.421	7.1
AuCeSmMA	76	2.4 <sup>2</sup>	5.424	8.5

<sup>a</sup> Lattice parameter of  $\text{CeO}_2 = 5.412 \text{ \AA}$ , ionic radii:  $\text{Ce}^{4+} = 0.97 \text{ \AA}$ ;  $\text{Ce}^{3+} = 1.14 \text{ \AA}$ ;  $\text{Al}^{3+} = 0.535 \text{ \AA}$ ;  $\text{Sm}^{3+} = 1.079 \text{ \AA}$ .

<sup>b</sup> Estimated by HRTEM.

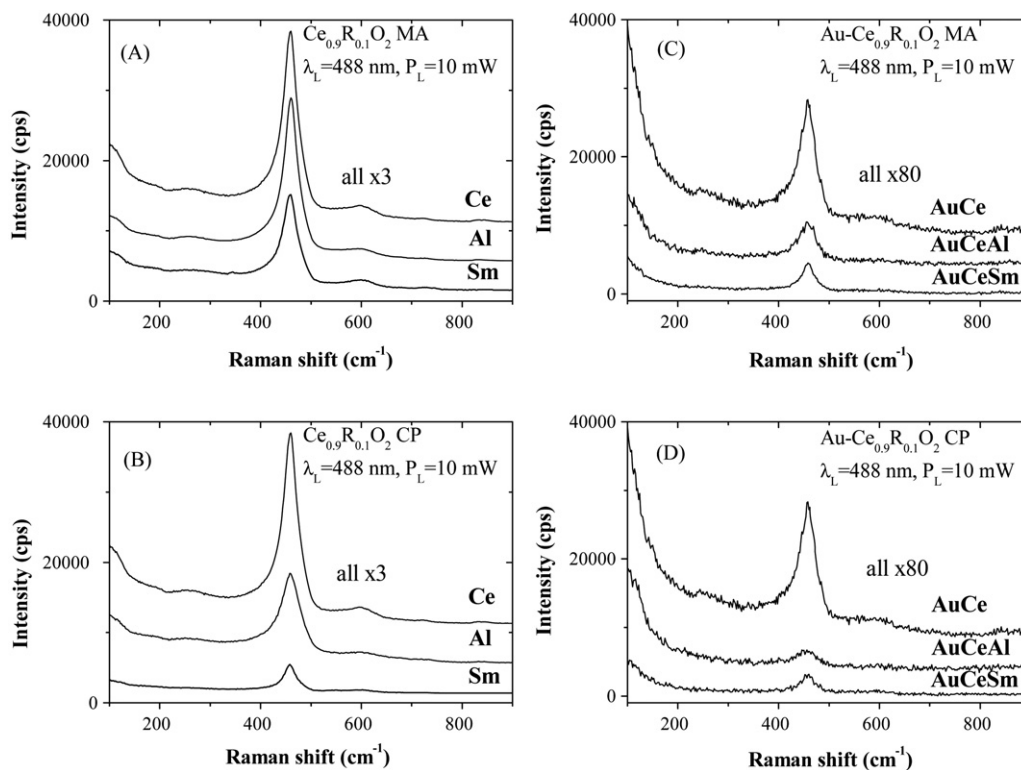


**Fig. 5.** Raman spectra of the initial supports: MA (A) and CP (B) and gold containing catalysts: MA (C) and CP (D).

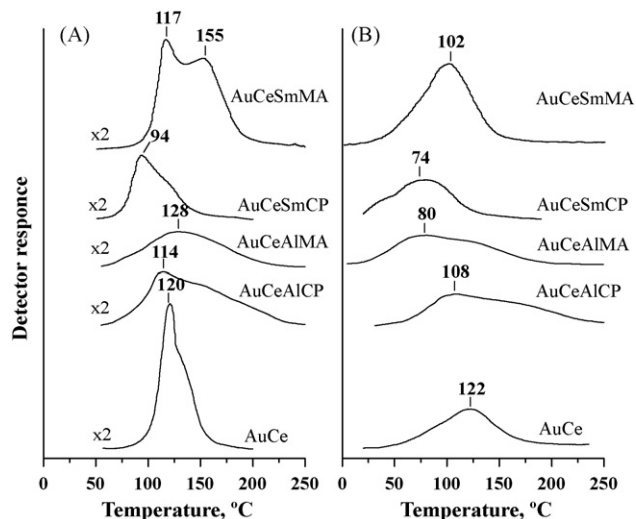


**Fig. 6.** TPR of studied catalysts: (A) fresh catalysts and (B) after reoxidation at 200 °C.

tance for the catalytic reaction studies. The complex LT TPR peaks can be related to the reduction of surface ceria layers and partially to the oxygen species coordinated around small gold particles. It is seen that the TPR peaks for the mixed  $\text{Me}^{3+}$ /ceria support are much broader than the narrow TPR peak of unpromoted AuCe sample. The  $T_{\text{max}}$  of the first peak in the TPR profile registered for the AuCeSmCP sample is located at 94 °C, which is in accordance with the higher catalytic activity of this sample. After reoxidation at 200 °C the TPR profiles exhibit also a complex character and the  $T_{\text{max}}$  of the TPR peaks shifts to lower values. This trend corresponds to the increase of the WGS activity after reactivation at the same temperature in air. Again, the lowest  $T_{\text{max}}$  was recorded for the AuCeSmCP sample, which exhibits the highest WGS activity. In order to compare quantitatively the TPR peaks' intensities as indicative for the oxygen

**Table 2**  
Full width at half maximum (FWHM) of the dominant ceria line in the Raman spectra.

Samples	FWHM ( $\text{cm}^{-1}$ )
AuCe	13.5
AuCeAlCP	48.5
AuCeAlMA	39.4
AuCeSmCP	32.3
AuCeSmMA	29.8

**Table 3**

Hydrogen consumption corresponding to the first TPR peak in the spectrum of fresh catalysts and after reoxidation at 200 °C.

Samples	Hydrogen consumption in direct TPR spectra ( $\mu\text{mol}$ )	Hydrogen consumption after reoxidation ( $\mu\text{mol}$ )
AuCe	23.1	15.2
AuCeAlCP	26.4	18.0
AuCeAlMA	17.6	16.1
AuCeSmCP	29.5	18.9
AuCeSmMA	35.9	27.9

capacity of the catalysts, the hydrogen consumption (HC) was calculated. The data are presented in Table 3. In all cases the hydrogen consumption is higher than that for the unpromoted AuCe. Comparing the  $\text{Me}^{3+}$  doped samples, the higher HC was calculated for the Sm doped catalysts. The lowest HC was found for the AuCeAlMA sample. After reoxidation, the HC does not fully recover the oxygen capacity, but remains higher for the Sm doped catalysts.

The catalysts were characterized by means of XPS as well. Fig. 7 shows the Au 4f XPS spectra taken from Sm doped samples CP and MA both fresh and spent, respectively. The most important data determined from the XPS spectra, like the binding energy (BE), atomic concentration (AC) of selected components and the XPS spectra fitting-data are presented in Table 4 for both Sm and Al doped catalysts, respectively. The Au 4f XPS spectra of the fresh samples were fitted successfully with two components, the first one at a BE of the Au  $4f_{7/2}$  close to the metallic gold ( $84 \pm 0.2$  eV) and the second one at the BE shifted to higher values (85–86 eV). However, after the catalytic processing (spent samples) only metallic gold was registered. The component with higher BE we assigned to positively charged, very small gold particles. Careful analysis of the Ce 3d XPS spectra allows distinguishing the relative contribution of the  $\text{Ce}^{3+}$  and  $\text{Ce}^{4+}$  compounds. The AC % of  $\text{Ce}^{3+}$  is a useful indicator of the ceria modification by the loaded dopants. The rough analysis indicates that these values are relatively high for all of the studied

**Table 4**

XPS data of gold-supported catalysts, fresh and spent.

Catalyst	Au $4f_{7/2}$		Ce $3d_{5/2}$ ( $\text{Ce}^{3+}$ )	
	Peak position (eV)	at.%	Peak position (eV)	at.%
AuCe fresh	84.70	0.56	885.36	5.12
	85.90	0.12	880.25	0.54
AuCe spent	84.15	0.45	886.04	3.37
			879.13	0.43
AuCeAlCP fresh	84.14	0.31	884.99	3.12
	85.69	0.07	880.23	0.76
AuCeAlCP spent	84.04	0.35	885.11	3.32
			879.83	0.80
AuCeAlMA fresh	84.24	0.29	885.78	2.88
	85.77	0.06	879.90	0.42
AuCeAlMA spent	84.27	0.34	886.09	3.28
			879.38	0.32
AuCeSmCP fresh	84.45	0.44	885.71	4.93
	85.61	0.29	880.40	1.28
AuCeSmCP spent	84.07	0.47	886.39	4.06
			879.49	0.96
AuCeSmMA fresh	84.25	0.11	885.85	2.70
	85.91	0.15	880.08	0.73
AuCeSmMA spent	84.17	0.24	885.96	2.84
			880.04	0.54

catalysts (see Table 4). There is no distinct dependence between the amount of  $\text{Ce}^{3+}$  and the type of dopant and preparation methods in the fresh and spent catalysts. It should be noted, however, that in the AuCeSmCP sample the AC% of  $\text{Ce}^{3+}$  is the highest for the fresh sample and remains very high also after the catalytic operation. This is in agreement with the highest WGS activity of this catalyst after reoxidation.

The FT-IR spectra of the activated AuCeSmCP and AuCeAlCP catalysts are shown in Fig. 8. The spectra of both samples in the  $\nu(\text{OH})$  stretching region display a sharp band at  $3655\text{ cm}^{-1}$  characteristic of OH species (type II) bridging two cerium sites, respectively [18]. The weak absorptions at  $3780\text{ cm}^{-1}$  (AuCeAlCP) and  $3755\text{ cm}^{-1}$

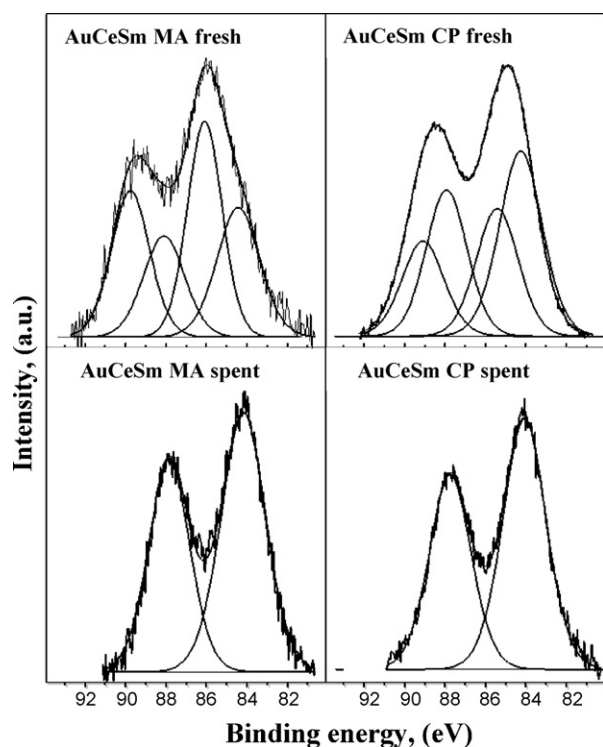


Fig. 7. Experimental and fitted Au 4f XPS spectra of studied catalysts: fresh and spent.

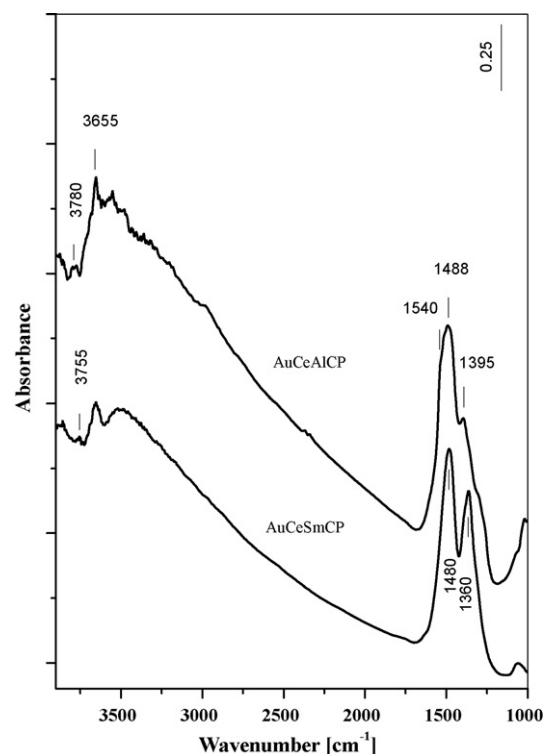
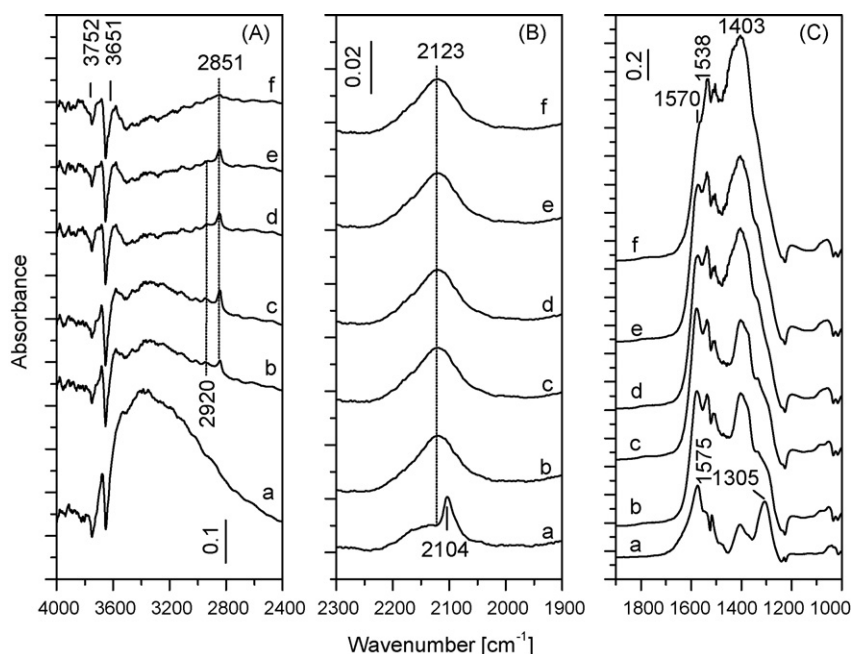


Fig. 8. FT-IR spectra of the activated AuCeSmCP and AuCeAlCP catalysts.



**Fig. 9.** FT-IR spectra collected during the exposure of the AuCeSmCP sample to a (10 mbar CO + 1 mbar H<sub>2</sub>O) mixture at 25 °C (a), 150 °C (b), 200 °C (c), 250 °C (d), 300 °C (e) and 350 °C (f).

(AuCeSmCP) most likely are due to isolated OH groups coordinated to Al<sup>3+</sup> and Sm<sup>3+</sup> sites, respectively. The broad absorption between 3600 and 3000 cm<sup>-1</sup> correspond to hydroxyls attached to reduced ceria [18]. The bands in the 1800–1000 cm<sup>-1</sup> region indicate the presence of residual nitro-nitrate and carbonate-carboxylate structures originating from the precursors used for sample preparation.

Fig. 9 presents the spectra obtained after the introduction to the IR cell of a gas mixture containing 10 mbar of CO and 1 mbar of H<sub>2</sub>O followed by heating of the isolated IR cell for 15 min at various temperatures. The strong absorption in the 3600–2500 cm<sup>-1</sup> region observed in the spectrum of the AuCeAlSm sample (Fig. 9A) taken at room temperature (spectrum a) is associated with the increased hydroxyl coverage. Negative bands at 3752 and 3651 cm<sup>-1</sup> are detected indicating that during the CO + H<sub>2</sub>O adsorption the isolated OH groups are either converted into H-bonded hydroxyls or involved in interaction with CO. The broad, unresolved band at approximately 2125 cm<sup>-1</sup> (Fig. 9B, spectrum a) corresponds to the forbidden <sup>2</sup>F<sub>5/2</sub> → <sup>2</sup>F<sub>7/2</sub> electronic transition of surface and subsurface Ce<sup>3+</sup> ions [8,19]. The appearance of this signal shows that the surface of the activated sample is reduced additionally upon exposure to the CO + H<sub>2</sub>O mixture at room temperature. The absorption at 2105 cm<sup>-1</sup> is characteristic of CO adsorbed on Au<sup>0</sup> [8,20,21]. The appearance of complex absorption bands in the 1900–1000 cm<sup>-1</sup> region indicates the formation of several OCO- containing species (Fig. 9C). The absence of a signal at 1630–1595 cm<sup>-1</sup> [18] attributable to the δ(HOH) bending suggests that the adsorbed water undergoes dissociative adsorption already at room temperature.

The increase in the temperature to 150 °C (Fig. 9A, spectrum b) causes strong decrease in the amount of H-bonded OH groups and emergency of a weak band at 2851 cm<sup>-1</sup> which in agreement with the literature [8,22] is assigned to the ν(CH) mode of adsorbed formate species. The surface concentration of the formate species reaches maximum at 200 °C (Fig. 9A, spectrum c) and decreases significantly at 350 °C. As proposed in earlier studies [23–26] the formate species are generated by a reaction of CO with the bridging OH groups on ceria. The spectra in Fig. 9A show that the intensities of the negative bands at 3752 and 3651 cm<sup>-1</sup> do not recover after the complete disappearance of the H-bonded hydroxyls, which con-

firms that these two types of isolated OH groups are involved in the formate formation. As with the other metals of group IB, the adsorption of CO on Au<sup>0</sup> is weak [27] and most likely, the Au<sup>0</sup>-CO species are no longer present in the spectra taken at higher temperatures. The intensity of the band at 2123 cm<sup>-1</sup>, corresponding to the Ce<sup>3+</sup> electronic transition, increases at 150 °C (Fig. 9B, spectrum b) and indicates that the amount of reduced cerium sites has increased. The intensity of this signal does not change considerably between 150 and 350 °C suggesting that there are Ce<sup>3+</sup> ions in the bulk of the crystallites. The strong increase in the absorption in the 1900–1000 cm<sup>-1</sup> region with increase in the temperature is caused by additional formation of formate and (bi)-carbonate species adsorbed on the support (Fig. 9C). Due to the complexity of these absorption bands, it is difficult to propose unambiguous interpretation.

The spectra recorded during the exposure of the AuCeAlCP catalyst to the CO + H<sub>2</sub>O mixture (10 mbar CO + 1 mbar H<sub>2</sub>O) at various temperatures are shown in Fig. 10. The following differences between the AuCeSmCP and AuCeAlCP catalysts can be noticed:

1. The absence of negative band in the OH stretching region in the spectrum taken at room temperature suggests that the water adsorbs molecularly on the AuCeAlCP sample (Fig. 10A, spectrum a). This is confirmed by the presence of a band at 1630 cm<sup>-1</sup> corresponding to δ(HOH) bending mode (Fig. 10C, spectrum a).
2. The broad, unresolved absorption detected at room temperature in the 2300–1900 cm<sup>-1</sup> region (Fig. 10B, spectrum a), which extends down to 1950 cm<sup>-1</sup>, is attributed to overlapping bands due to the electronic transition of Ce<sup>3+</sup> [19], Au<sup>0</sup>-CO and Au<sup>δ-</sup>-CO species [8,20,21]. Such low-frequency tail is not seen in the spectrum of AuCeSmCP (Fig. 9B, spectrum a) indicating that Au<sup>δ-</sup> species do not exist on the surface of this catalyst. The absence of a distinct Au<sup>0</sup>-CO band in the case of the AuCeAlCP catalyst suggests lower dispersion of the gold particles as compared with the Sm-containing sample, which is in agreement with the HRTEM results [3].
3. The amount of the formate species generated on the AuCeAlCP sample is significantly lower than that observed on the AuCeSmCP catalyst and they display higher thermal stability.

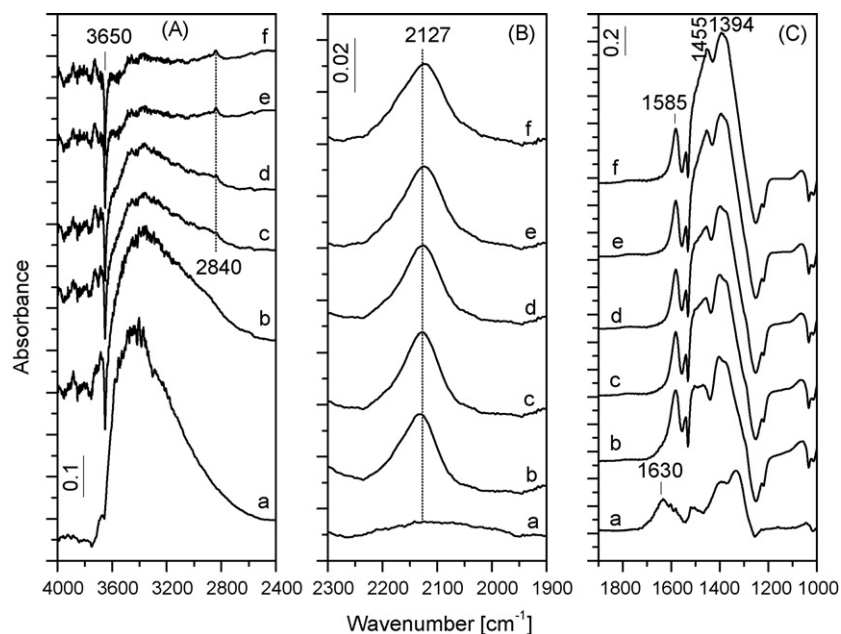


**Fig. 10.** FT-IR spectra collected during the exposure of the AuCeAlCP sample to a (10 mbar CO + 1 mbar H<sub>2</sub>O) mixture at 25 °C (a), 150 °C (b), 200 °C (c), 250 °C (d), 300 °C (e) and 350 °C (f).

As with the AuCeSmCP catalyst, the amount of Ce<sup>3+</sup> sites increases at 150 °C and does not change considerably up to 350 °C (Fig. 10B). The low-frequency tail of the complex absorption between 2300 and 1900 cm<sup>-1</sup> disappears at 150 °C (Fig. 10B, spectrum b). This fact supports the suggestion made above that CO adsorbed on metallic gold has low thermal stability. The appearance of strong bands in the 1900–1000 cm<sup>-1</sup> region with the increase in the temperature is associated with the formation of several carbonate–carboxylate structures (Fig. 10C).

#### 4. Discussion

The experimental data presented above show that the WGS activity depends on the nature of Me-dopants applied and on the preparation methods. Obviously, the WGS activity is affected by the preparation method in the case of Al doped ceria catalysts. The AuCeAlMA sample exhibits higher activity than the corresponding CP sample. Oxygen vacancies, created during CP preparation method, are formed deeper into the bulk of ceria and the oxidation capacity of water is too low to re-oxidize the catalysts surface. The MA preparation method leads mainly to surface modification of the Al doped catalysts. Thus, during the WGS reaction, water is able to re-oxidize the catalysts' surface more effectively. Quite different WGS reaction course is observed for the Sm doped catalysts. Both samples, CP and MA, show similar activities, especially, after the reoxidation and even the CP catalysts increase their WGS activity slightly. These differences in the catalytic behaviour of the studied catalysts can be explained by the differences in the structure and properties of the samples. As it was already shown, the ionic radius of Sm(III) is close to that of Ce(IV) and much higher than that of Al(III) (see Table 1). Therefore, the Sm contribution to the ceria support does not cause change in the lattice parameters [17]. In the case of Al doped CP samples, the Al atoms occupy the interstitial positions in ceria crystallites which leads to contraction of the lattice. In the MA samples the Al dopant is located on the surface and its contraction effect on the lattice is low. As a result, the difference in the *a* parameter of the CP and MA samples doped by Al becomes significant. More defective struc-

ture can also be found analyzing the Raman spectra. The FWHM calculated for the Al doped catalysts is much higher for the CP than for the MA sample. For the Sm doped samples these values are lower (see Table 2), which can indicate that the oxygen vacancies are located around Sm and the ceria structure is better ordered. The relatively high HC of the Sm-containing sample is a result of the large number of vacancies that are not located in the ceria structure. After the reoxidation, the oxygen capacity is not fully recovered, but remains higher than that of the Al doped catalysts. The model proposed by some of us [2] considering Au<sup>δ+</sup>V<sub>o</sub>Ce<sup>3+</sup> as the active sites of WGS reaction, illustrated the initial state. However a dynamic redox process occurs during the catalytic reaction, leading to electron transfer from Ce<sup>3+</sup> to gold. The result is formation of Ce<sup>4+</sup> and Au<sup>0</sup> and even Au<sup>δ-</sup>. Contrary to the Au<sup>δ+</sup>V<sub>o</sub>Ce<sup>3+</sup>, the available Au<sup>δ+</sup>V<sub>o</sub>Al<sup>3+</sup> and Au<sup>δ+</sup>V<sub>o</sub>Sm<sup>3+</sup> sites in the catalysts are not active in the WGS reaction [2] (V<sub>o</sub> stays for oxygen vacancy). In the case of Sm, the HC after the reoxidation at 200 °C is low, but most likely it is sufficient to re-oxidize the Ce<sup>3+</sup>V<sub>o</sub> species, which are part of the active sites. The reoxidation of Ce<sup>3+</sup>V<sub>o</sub> is enhanced by the close contact with the small gold particles. Therefore, the WGS activity of the AuCeSmCP sample increases after reoxidation. However, in this case probably not the whole surface is fully re-oxidized, but only part of the surface containing the active sites. This interpretation can be useful to explain the observed relationship between the WGS activity and the method of preparation, as well as the nature of dopant applied.

The results of the in situ FT-IR investigation of the CO + H<sub>2</sub>O adsorption on AuCeAlCP and AuCeSmCP catalysts show that there are differences between both catalysts. The presence of low-frequency tail in the carbonyl region of the room temperature spectrum of AuCeAlCP sample (Fig. 9B, spectrum a) has been associated with the formation of carbonyl species involving Au<sup>δ-</sup> sites. This indicates that the oxygen vacancies are present around the gold particles allowing an electron transfer to occur that results in the Au<sup>δ-</sup> species [8,20,21]. The lack of signal between 2050 and 1950 cm<sup>-1</sup> in the spectrum of AuCeSmCP confirms the conclusion made above that in the Sm doped sample the oxygen vacancies are adjusted around the Sm atoms.

The mechanisms of WGS reaction over gold catalysts have been summarized and discussed in the recent reviews of Burch [28] and Bond [29]. Two main types of mechanism have been proposed: the redox mechanism and associative mechanism. Both mechanisms start with dissociation of water on the catalyst surface. The subsequent step in the redox mechanism involves the dissociation of hydroxyl, whereas the associative mechanism occurs through the intermediacy of formate, carbonate or carboxylate species. The main WGS pathway remains still unclear and according to Burch [28], the dominant mechanism will depend on the type of the catalyst and the experimental conditions. As shown in Figs. 9 and 10, the amount of formate species generated on the AuCeSmCP is higher than that on the AuCeAlCP catalyst. Although the experimental conditions of the FT-IR measurements and catalytic test are different, the higher concentration of the formate species on the Sm-containing sample parallels its higher activity. The results of recent DRIFTS-SSITKA study on Au/Ce(La)O<sub>2</sub> catalyst [30], however, do not prove that the main reactive intermediates leading to the formation of CO<sub>2</sub> are the formate species. We do not attempt to make conclusions about the mechanism of WGS reaction over the AuCeAlCP and AuCeSmCP catalysts from the obtained in situ FT-IR results. It should be noted, however, that the better catalytic performance of the AuCeSmCP catalyst could be related to its ability to ensure sufficient concentration of specific (highly reactive) formate species, which are located at the interface between the Au particles and ceria-samarium support and which cannot be detected. As proposed by Behm and coworkers for Au/CeO<sub>2</sub> [31], the formate species are generated on the Au-support interface. Because the number of these active sites is low, their ability to accommodate the formate species is limited. As a result of this, the formates spillover onto the support. There is a dynamic equilibrium between the mobile formate species located on the support (which is associated with the IR intensity of the formate band) and formates adsorbed at Au-support interface [31]. Most likely, the high activity of AuCeSmCP catalyst could be related with the high dispersion of Au nanoparticles leading to large number of active Au-support interface sites (Au<sup>δ+</sup>V<sub>o</sub>Ce<sup>3+</sup> as proposed above), which results in high concentration of formate species.

According to the FT-IR data, the AuCeSmCP and AuCeAlCP samples behave differently with regard to the adsorption of water at room temperature: water adsorbs dissociatively on the former catalyst and molecularly adsorbed water has been observed on the Al doped sample. It can be proposed that the higher concentration of Au<sup>δ+</sup>V<sub>o</sub>Ce<sup>3+</sup> sites on the surface of the AuCeSmCP catalyst facilitates the dissociation of water and supports the active role of defective ceria in the latter process. This conclusion agrees with the results of DFT-GGA calculations of Liu and Rodriguez [32] which show that ceria is involved directly in the WGS reaction by lowering the barrier of water dissociation. The facile dissociation of water on the AuCeSmCP catalyst could account also for its better performance in the WGS reaction.

## 5. Conclusions

Gold catalysts supported on ceria doped by Sm and Al were synthesized. The supports were prepared using two different methods with the aim to modify ceria by different extend. The CP preparation techniques applied makes defects in the structure of ceria involving formation of oxygen vacancies that are located within the bulk of ceria. The MA method leads only to surface modification of the prepared sample. The WGS activity is found to be different for Al doped catalysts prepared by CP and MA techniques, respectively. In the case of Sm doped Au catalysts, practically, no difference has been found between the CP and MA samples in the WGS activity. In the CP sample doped by Al the vacancies are located within the

bulk ceria structure, whereas in the AuCeSmCP sample the vacancies are located most likely around Sm and the ceria structure seems to be better ordered than the Al doped ceria. The AuCeSmCP sample shows the lowest temperature  $T_{\max}$  in the TPR profiles which could be related to the higher WGS activity of this sample. However, there is no distinct correlation between the reducibility and WGS activity of the studied catalysts. The Au 4f XPS spectra taken from fresh samples reveal higher contribution of dispersed form of Au (the XPS Au states characterized by higher BE) for Sm doped catalysts than for the corresponding Al doped samples. The Ce 3d XPS spectra disclose also a higher concentration of Ce<sup>3+</sup> evaluated before the catalytic operation for Sm doped catalysts as compared with the Al doped fresh samples. These observations agree well with the model of active sites for the WGS reaction (Au<sup>δ+</sup>V<sub>o</sub>Ce<sup>3+</sup>, where V<sub>o</sub> is an oxygen vacancy), which we proposed recently [2]. The amount of formate species observed on the AuCeSmCP is higher than that on the AuCeAlCP catalyst and parallels the catalytic activity. The high activity of AuCeSmCP catalyst could be related with the high dispersion of Au nanoparticles leading to large number of active Au-support interface sites (Au<sup>δ+</sup>V<sub>o</sub>Ce<sup>3+</sup>), which results in high concentration of formate species. The higher concentration of Au<sup>δ+</sup>V<sub>o</sub>Ce<sup>3+</sup> sites on the surface of the AuCeSmCP catalyst facilitates the dissociation of water. This could account also for the better performance of the Sm doped catalyst in the WGS reaction. The Sm and Al dopants are not active in catalytic reaction; they increase only the oxygen mobility and improve the stability of the catalysts, preventing the gold and ceria particles from agglomeration.

## Acknowledgements

This work has been performed in the framework of a D36/003/06 COST program and was also supported by the National Science Fund at the Ministry of Education and Science of Bulgaria, project TK-X-1709.

## References

- [1] D. Andreeva, V. Idakiev, T. Tabakova, L. Ilieva, P. Falaras, A. Bourlinos, A. Travlos, *Catal. Today* 72 (2002) 51.
- [2] D. Andreeva, I. Ivanov, L. Ilieva, J.W. Sobczak, G. Avdeev, K. Petrov, *Top. Catal.* 44 (2007) 173.
- [3] D. Andreeva, I. Ivanov, L. Ilieva, M.V. Abrashev, R. Zanella, J.W. Sobczak, W. Lisowski, M. Kancheva, G. Avdeev, K. Petrov, *Appl. Catal. A: Gen.* 357 (2009) 159.
- [4] T. Luo, J.M. Vohs, R.J. Gorte, *J. Catal.* 210 (2002) 397.
- [5] P. Panagiotopoulou, D. Kondarides, *Catal. Today* 112 (2006) 49.
- [6] P. Panagiotopoulou, J. Papavasiliou, G. Avgouropoulos, T. Ioannides, D.I. Kondarides, *Chem. Eng. J.* 134 (2007) 16.
- [7] M.S. Chen, D.W. Goodman, *Catal. Today* 111 (2006) 22, references therein.
- [8] T. Tabakova, F. Boccuzzi, M. Manzoli, D. Andreeva, *Appl. Catal. A: Gen.* 252 (2003) 385.
- [9] W. Kraus and G. Nolze, "PowderCell for Windows, Version 2.4", Federal Institute for Materials Research and Testing, Rudower Chaussee 5, 12489 Berlin, Germany, 1984.
- [10] N. Kotzev, D. Shopov, *J. Catal.* 22 (1971) 297.
- [11] D.A.M. Monti, A. Baiker, *J. Catal.* 83 (1983) 323.
- [12] M. Romeo, K. Bak, J. El Fallah, F. Le Normand, *Surf. Interface Anal.* 20 (1993) 508.
- [13] L. Armelao, D. Barecca, G. Bottaro, A. Gasparotto, E. Tondello, *Surf. Sci. Spectra* 8 (2001) 247.
- [14] A.Q. Wang, P. Punaichapetch, R.M. Wallace, T.D. Golden, *J. Vac. Sci. Technol. B* 21 (2003) 1169.
- [15] G.W. Graham, W.H. Weber, C.R. Peters, R. Usmen, *J. Catal.* 130 (1991) 310.
- [16] I. Kosacki, T. Suzuki, H.U. Anderson, Ph. Colomban, *Solid State Ionics* 149 (2002) 99.
- [17] A. Trovarelli, "Catalysis by Ceria and Related Materials", *Catal. Sci. Series v.2*, Ser. Ed. G. Hutchings, Imp. College Press, London, 2002, p. 37.
- [18] C. Binet, M. Daturi, J.-C. Lavalley, *Catal. Today* 50 (1999) 207.
- [19] C. Binet, A. Bardi, J.-C. Lavalley, *J. Phys. Chem.* 98 (1994).
- [20] T. Tabakova, F. Boccuzzi, M. Manzoli, J.W. Sobczak, V. Idakiev, D. Andreeva, *Appl. Catal. A* 298 (2006) 127.
- [21] T. Tabakova, F. Boccuzzi, M. Manzoli, J.W. Sobczak, V. Idakiev, D. Andreeva, *Appl. Catal. B* 49 (2004) 73.
- [22] G. Busca, J. Lamotte, J.-C. Lavalley, V. Lorenzelli, *J. Am. Chem. Soc.* 109 (1987) 5197.
- [23] T. Shido, Y. Iwasawa, *J. Catal.* 136 (1992) 493.

- [24] T. Shido, Y. Iwasawa, *J. Catal.* 141 (1993) 71.
- [25] G. Jacobs, B.H. Davis, *Appl. Catal. A* 284 (2005) 31.
- [26] G. Jacobs, B.H. Davis, *Appl. Catal. A* 284 (2005) 499.
- [27] A. Davidov, in: N.T. Sheppard (Ed.), *Molecular Spectroscopy of Oxide Catalyst Surfaces*, Wiley, 2003, p. 274.
- [28] R. Burch, *Phys. Chem. Chem. Phys.* 8 (2006) 5483.
- [29] G. Bond, *Gold Bull.* 42 (2009) 337.
- [30] F.C. Meunier, D. Reid, A. Gouet, S. Shekhtman, C. Hardcare, R. Burch, W. Deng, M. Flytzani-Stephanopoulos, *J. Catal.* 247 (2007) 277.
- [31] R. Leppelt, B. Schumacher, V. Plzak, M. Kinne, R.J. Behm, *J. Catal.* 244 (2006) 137.
- [32] P. Liu, J.A. Rodriguez, *J. Chem. Phys.* 126 (2007) 164705.